

A Pre-Merger Stage Galaxy Cluster: Abell 3733

H. İlker KAYA,¹ Turgay CAGLAR,^{1,2*} Hakan SERT^{1,3}

¹*Yıldız Technical University, Faculty of Science and Art, Department of Physics, Istanbul 34220, Turkey*

²*Leiden University, Leiden Observatory, Astronomy Department, Leiden, 2380RA, The Netherlands*

³*von Karman Institute for Fluid Dynamics, Chaussée de Waterloo, 72, B-1640 Rhode-St-Genèse, Belgium*

Accepted XXX. Received YYY; in original form ZZZ

ABSTRACT

The galaxy cluster Abell 3733 (A3733) is a very suitable candidate in addressing dynamical processes throughout galaxy cluster mergers. This study shows structural analysis results of A3733 ($z = 0.038$) based on X-ray and optical data. According to X-ray luminosity map, A3733 hosts two sub-structures separated in the sky by ~ 0.25 Mpc, and the two distinct clumps are located in the East (A3733E) and the West (A3733W) directions. Both sub-structures are centred on two different brightest cluster galaxies (BCGs), and the X-ray and optical centroids of both BCGs substantially coincide with each other. The intracluster medium (ICM) temperatures of the sub-structures are estimated to be 2.79 keV for A3733E and 3.28 keV for A3733W. Both sub-structures are found to be hosting cool central gas ($kT \sim 1.5$ –2.5 keV) surrounded by hotter gas ($kT \sim 3.0$ –3.5 keV). Besides, the X-ray concentration parameters are found to be $c \sim 0.3$ for each sub-structure. These results indicate the existence of cool centres for both sub-structures. The optical density map reveals a crowded galaxy population within the vicinity of A3733W. The high probable (% 88.2) dynamical binding model of A3733 suggests that the cores of sub-structures have a 3D separation of 0.27 Mpc and will collide in 0.14 Gyr with the relative in-falling velocity of 1936 km s^{−1}. As a conclusion, this study demonstrates some evidence suggesting that the A3733 system is in the pre-merger state.

Key words: X-rays: galaxies: clusters – galaxies: clusters: general – galaxies: clusters: individual: Abell 3733 – galaxies: clusters: intracluster medium

1 INTRODUCTION

Clusters of galaxies are the largest cosmic laboratories in which evolution of the universe can be studied in detail. They are formed by virtue of in-falling of the other objects through a central dominant object by the gravitational attraction (Press & Schechter 1974). One of the most crucial results of gravitational attraction is galaxy clusters mergers, which are the most energetic ($\sim 10^{64}$ ergs) events in the universe (Sarazin 2002). Numerical simulations also demonstrate that galaxy clusters are formed via accretion of sub-clusters along the filaments (e.g., West et al. 1991). Therefore, more detailed investigations of merging systems are essential for understanding the structural formation of the universe.

The theoretical concept of mergers is the angular momentum and energy transfer between the merging galaxy clusters (e.g., Sarazin 2002). The ICM temperature of vicinity of merging systems can be increased as a result of galaxy

cluster interactions. Mergers are able to stop the cooling flow and can also destroy (or relocate) cool centres of galaxy clusters (Markevitch et al. 2000; Markevitch & Vikhlinin 2007).

Optical and X-ray correlations have been very successful for explaining the dynamics of mergers. The optical and X-ray sub-clustering are found to be well-correlated for the majority of binary systems (e.g., Baier et al. 1996; Kolokotronis et al. 2001). X-ray investigations of the binary systems reported the existence of hot regions in-between sub-structures for many samples (Gutierrez & Krawczynski 2005; Sarazin et al. 2013; Kato et al. 2015; Akamatsu et al. 2016, 2017; Caglar & Hudaverdi 2017; Caglar 2018; Botteon et al. 2018; Hallman et al. 2018). But, the origin of hot region between the merging sub-structures was proposed by the different mechanisms, such as shock-heating or adiabatic compression (Takizawa 1999; Zuhone et al. 2011; Schmidt et al. 2017). On the other hand, some merging binary galaxy clusters with higher separations did not show a strong evidence for shock heating (e.g., Fujita L. et al. 1996, 2008; Werner et al. 2008). The extended radio emissions, such as radio halo and relics, are proposed to be generated by the

* E-mail: caglar@strw.leidenuniv.nl

turbulence after the collisions between the cores; therefore, they are not observed in the pre-merging binary galaxy clusters (Feretti L. et. al, 2002, 2012).

X-ray analysis of A3733 was performed with ROSAT data by Ebeling et al. (1996) resulting in $kT = 2.2$ keV and $L_x = 4.2 \times 10^{43}$ erg s $^{-1}$. Then, Piffaretti et al. (2011) used ROSAT data to measure cluster's mass and luminosity at the overdensity of 500 and provided the following results: $r_{500} = 678.9$ kpc, $L_{500} = 2.8 \times 10^{43}$ erg s $^{-1}$, and $M_{500} = 9.2 \times 10^{13}$ M_{\odot} . A3733 is a Bautz-Morgan type I-II galaxy cluster with richness class $R = 1$ (Robertson & Roach (1990)) and redshift $z = 0.038$ (Dalton et al. 1994; Solanes & Stein 1998; Smith et al. 2004). The kinematic investigations of A3733 were performed by Stein (1996, 1997) and Solanes & Stein (1998); however, neither result demonstrated significant substructure within the cluster's potential well. NGC 6999 is classified as the brightest cluster galaxy (BCG) of A3733 by Postman & Lauer (1995), and in the same work, the second brightest galaxy of A3733 is reported to be NGC 6998 with a slight absolute magnitude difference $\Delta M = 0.013$.

This study, which reports an optical and X-ray investigation of merging galaxy cluster A3733, aimed to understand the physical structure of A3733 using X-ray and optical comparison. Dynamical events of A3733 occurred by mergers are also discussed in the present study, which is organised in the following manner: Section 2 presents the observation logs and data processing; Section 3 describes X-ray and optical data analysis procedures; Section 4 explains the Newtonian gravitational binding criterion of two-body systems; Section 5 covers the discussion of our results and finally, we summarise our results in section 6. We adopt in this paper a standard Λ CDM cosmology parameters: $H_0 = 70$ km s $^{-1}$ Mpc $^{-1}$, $\Omega_M = 0.3$ and $\Omega_{\Lambda} = 0.7$ for a flat universe. In this cosmology, $1'$ corresponds to 44.48 kpc. Unless stated otherwise, the error values are quoted at the % 90 confidence interval in our analysis.

2 OBSERVATIONS AND DATA PROCESSING

The first *XMM-Newton* observation was performed on 2015 November 30 for exposure of 15.8 ks, and the second *XMM-Newton* observation was performed on 2016 December 8 for exposure of 18.5 ks. The medium filter was used for MOSs and pn cameras on the both observations. X-ray observations were taken in full frame for MOSs and extended full frame for pn. Suzaku satellite was also used to observe A3733 with 3×3 clocking mode on 2016 August 16 for exposure of 14.6 ks. The observation was performed with two front illuminated (FI) CCD chips (XIS 0 and XIS 3) and one back illuminated (BI) CCD chips (XIS 1). X-ray observational data were gathered from *XMM-Newton* Science Archive (XSA) and Suzaku Data Archive and Transmission System (DARTS). The log of observations are presented in Table 1. The first radio observation was performed at a frequency of 4850 Mhz on the Parkes-MIT-NRAO (PMN) survey (Wright et al. 1994). 1400 Mhz radio observation of A3733 was performed on the The NRAO VLA Sky Survey (NVSS) (Condon et al. 1998), and the last observation at the frequency of 150 Mhz was performed on the the GMRT all-sky radio survey (Intema et al. 2017). Radio images were gathered from Skyview archive.

Table 1. X-ray Observations.

ObsID	Satellite	Date Obs	Exposure (ks)
809108010	<i>Suzaku</i>	2016-08-16	14.6
0765000301	<i>XMM-Newton</i>	2016-12-08	18.5
0741580801	<i>XMM-Newton</i>	2015-11-30	15.8

For *XMM-Newton* data, we performed data reduction using *XMM-Newton* Science Analysis Software (*XMM-SAS v15.0* and *XMM-Newton* Extended Source Analysis Software (*XMM-ESAS*). Current calibration file (ccf) and summarised observation data file (odf) were created using the tasks: *cifbuild-4.8* and *odfingest-3.30*, respectively. The *emchain-11.19* and *epchain-8.75.0* tasks were applied to data, which generated MOS and pn event files, respectively. The light curve was generated to determine a final net data, and corrupted data was extracted performing *evselect-3.62*. Finally, point-like X-ray sources within the galaxy cluster were detected using *edetect_chain-3.14.1*, and the point sources are removed from data in our analysis. Suzaku data analysis were processed with *heasoft* version 6.21 and the latest calibration database (CALDB-2014-05).

3 ANALYSIS

3.1 Optical Analysis

We obtained spectroscopic redshifts of 89 galaxies within 1.5 Mpc radius of A3733 in the literature (Stein 1996; Katgert et al. 1998; Solanes & Stein 1998; Jones et al. 2009). Cluster membership were assigned with heliocentric velocities in the interval $10500 < V < 13000$ km s $^{-1}$. Cluster member galaxies were used to generate the projected galaxy density map of A3733, which is presented in Fig. 1 (top). The white and blue dots represent the position of BCGs and member galaxies, respectively. Moreover, we investigated the velocity histogram of A3733 using the cluster member galaxies (see Fig. 1 (bottom)). Cluster's mean redshift is demonstrated as a black dashed line, and the velocities of BCGs are pointed with the black arrows for visual aid. We also present the member galaxies of A3733 in Fig. 2, which clearly shows the a crowded region around BCG2.

3.2 Spatial Analysis

The *XMM-Newton* background subtracted, exposure and vignetting corrected, combined X-ray image was generated by the following analysis procedure. MOS and pn raw data were created by the *mos-filter* and *pn-filter* task respectively. For MOS and pn using *mos-spectra* and *pn-spectra*, *XMM-Newton* X-ray images were generated in the 0.4-10.0 keV energy range respectively. The point-like X-ray sources in A3733 were determined using the *cheese* task on the 5×10^{-15} erg cm $^{-2}$ s $^{-1}$ flux threshold. The *cheese* task provides the event, exposure and mask images that are used for excluding point-like sources for the further purposes. In our analysis, point-like sources are excluded from the data by using mask parameter, which was set to 1.Proton scale,

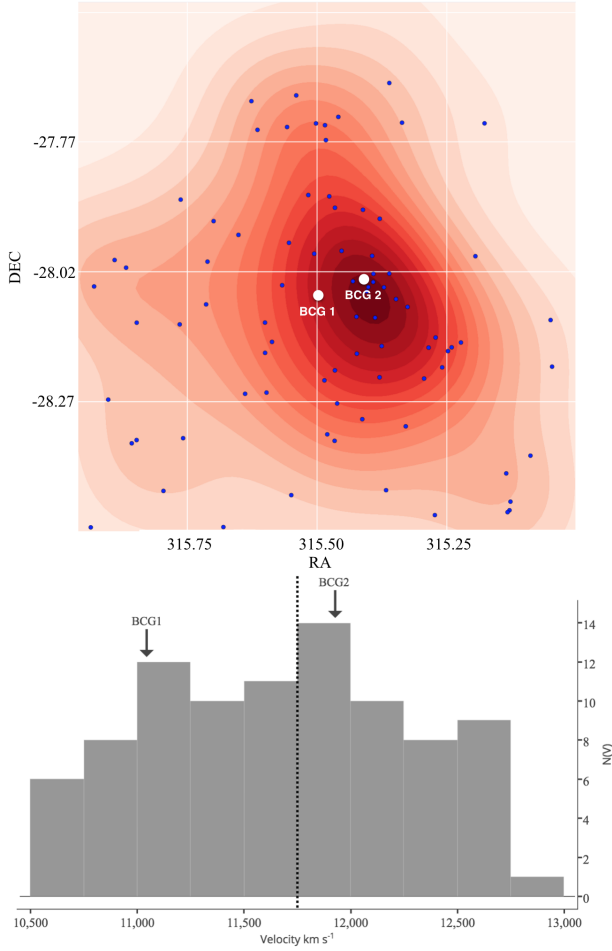


Figure 1. **Top:** The projected galaxy density map of A3733 within 1.5 Mpc radius of the field. The white and blue dots represent the position of BCGs and member galaxies, respectively. **Bottom:** Velocity histogram of A3733 (binning of 250 km s⁻¹) for 89 member galaxies. The black dashed line represents the mean velocity of A3733.

proton tasks were used for removing soft proton and background contamination from the data. Since the *XMM-ESAS* performs analysis within the detector coordinates, rot-im-det-sky task was used to convert the detector coordinates to celestial coordinates. Finally, MOS and pn data were combined by comb task, and the combined image was smoothed adaptively by the adapt task. The background subtracted, exposure and vignetting corrected, combined, and adaptive smoothed X-ray image is presented in Fig. 3.

The surface brightness is defined as projected plasma emissivity per area on the sky. The β model was used to fit the X-ray surface brightness of each sub-structures. (Cavaliere & Fusco-Femiano 1976). The model is defined as:

$$S(r) = S_0 \times [1 + (r/r_c)^2]^{-3\beta+0.5} + c, \quad (1)$$

where S_0 is the central surface brightness, r_c is the core radius, and β is the shape parameter. In this equation, c parameter was added to estimate the background level, and it is crucial to estimate best-fit parameters of the surface brightness. Whereas the background level is found to be

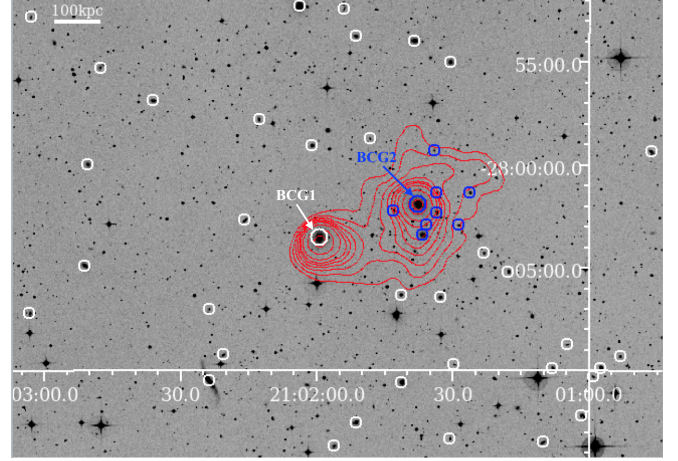


Figure 2. Optical DSS image of A3733, overlaid with X-ray contours. X-ray contours are generated using background subtracted, exposure and vignetting corrected, combined *XMM-Newton* image. The white and blue circles represent the member galaxies of A3733. Member galaxies within the ICM of A3733W are presented as blue circles for visual aid.

Table 2. The best-fit parameters of *XMM-Newton* data for β -model and r_{2500} .

Region	r_c (kpc)	β	r_{2500} (kpc)
A3733E	$8.27^{+2.79}_{-2.55}$	$0.46^{+0.065}_{-0.079}$	$429.8^{+54.6}_{-47.7}$
A3733W	$6.98^{+3.19}_{-2.50}$	$0.47^{+0.067}_{-0.081}$	$467.3^{+63.4}_{-53.7}$

$2.22 \pm 0.22 \times 10^{-2}$ counts arcsec⁻², the resulting β model parameters are presented in Table 2.

3.3 Spectral Analysis

The evselect-3.62 task was used to generate spectrum and background files for the spectral analysis of *XMM-Newton*. The response files for the A3733 galaxy were generated using the rmfgen-2.2.1 and arfgen-1.92 tasks. The local background was removed from the source file using an annular region within 11' - 12' away from the cluster center. The instrumental background lines such as Al K- α , Si K- α and Cu K- α were carefully removed from the data. The spectrum files of *Suzaku* was created by XSELECT-2.4. Non X-ray background (NXB) was subtracted from spectra by the background file, which was generated by xisnxbgen-2010-08-22. The Cosmic X-ray background (CXB) were modelled with a photon index of 1.4 (Hickox & Markevitch 2006). The xissimarfgen-2010-11-05 and xisrmfgen-2012-04-21 tasks were used to generate the response files. All generated spectral files were grouped by grppha. We perform the spectral analysis of A3733 using XSPEC-12.9.1 (Arnaud 1996). Thermal model APEC (Smith et al. 2001) and the X-ray absorption model (Wilms et al. 2000) TBABS were used in our analysis to estimate plasma temperature. The *XMM-Newton* data were simultaneously fitted within the energy range of 0.3 - 10.0 keV using 4 MOS and 2 pn data from

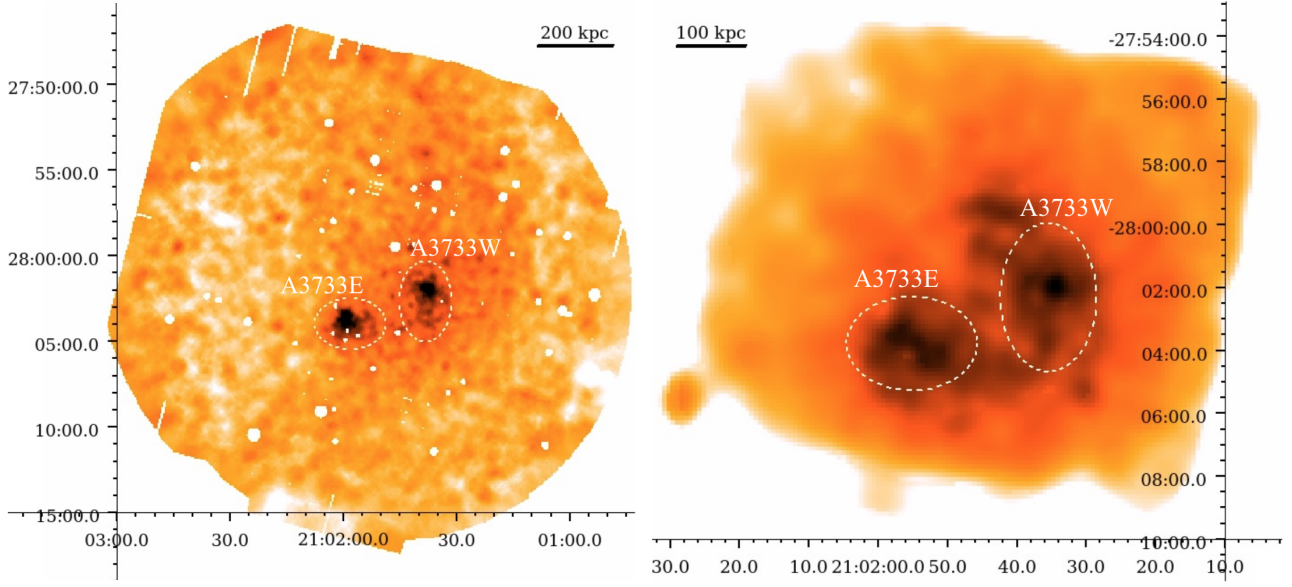


Figure 3. **Left:** The background subtracted, exposure and vignetting corrected, combined, and adaptive smoothed X-ray image within the energy range of 0.3 - 10 keV. **Right:** The combined and adaptive smoothed Suzaku raw X-ray image.

Table 3. The spectral best-fit parameters of A3733 with ¹*XMM-Newton* and ²*Suzaku* data.

Region	kT (keV)	Abundance (Z_{\odot})	χ^2/dof
A3733E ¹	$2.79^{+0.21}_{-0.22}$	$0.38^{+0.14}_{-0.12}$	2066/1831 = 1.12
A3733W ¹	$3.28^{+0.27}_{-0.25}$	$0.34^{+0.13}_{-0.11}$	2058/1856 = 1.11
Bridge ¹	$4.14^{+0.40}_{-0.51}$	$0.34^{+0.14}_{-0.13}$	1544/1350 = 1.14
A3733E ²	2.49 ± 0.41	$0.36^{+0.21}_{-0.15}$	297/351 = 0.85
A3733W ²	$3.12^{+0.46}_{-0.41}$	$0.27^{+0.23}_{-0.19}$	306/343 = 0.89
Bridge ²	$4.09^{+1.29}_{-0.95}$	0.3 (fix)	136/152 = 0.89

both *XMM-Newton* observations. The *Suzaku* data was also fitted simultaneously within the energy range of 0.8 - 7.0 keV using XIS0, XIS1 and XIS3 data. The spectral fit results of A3733 are presented in Table 3.

3.4 X-ray Morphological Parameters

X-ray morphological parameters are essential tools to resolve dynamical disturbance level of galaxy clusters. To understand the disturbance of each sub-structure of A3733, we estimated the centroid shift parameters for each one. In undisturbed galaxy clusters, the centroid shift are expected to be spherically symmetric and roughly equal to zero. We used the method provided by [Mohr et al. \(1995\)](#) in our centroid shift estimations. The centroid shift parameter can be obtained by the following equation:

$$w = \left[\frac{1}{N-1} \sum (\Delta_i - \langle \Delta \rangle)^2 \right]^{1/2} \times \frac{1}{R_{ap}}, \quad (2)$$

where N is the total aperture number, Δ is the separation between X-ray peak and the centroid of i th aperture, and R_{ap} is 500 kpc, which is decreased in steps of 5%.

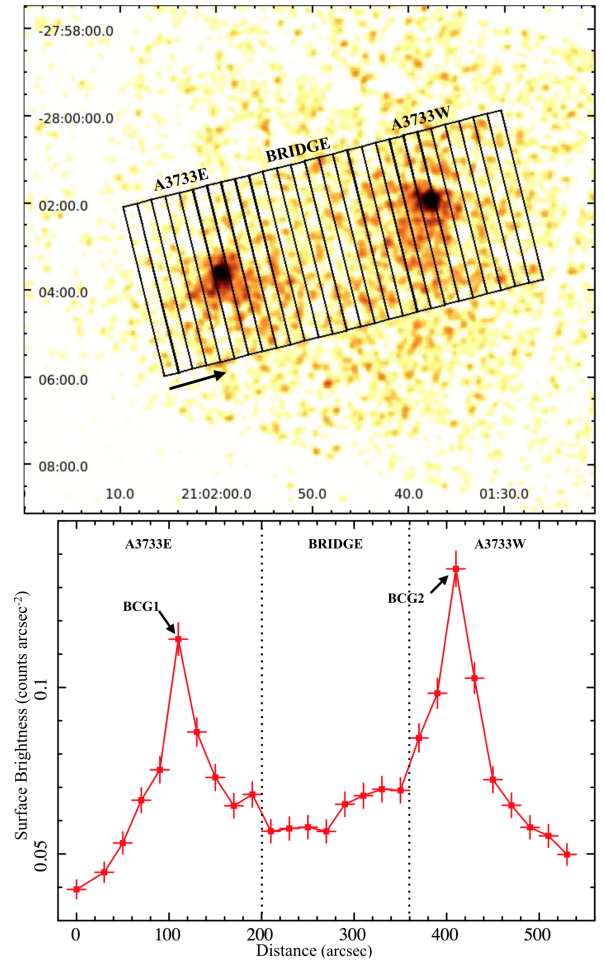


Figure 4. The surface brightness profile of the A3733 system demonstrating the absence of compressed gas between sub-structures.

Table 4. X-ray morphological parameters of A3733 obtained from *XMM-Newton* data. MD = Moderately Disturbed, CC = Non-cool core.

Cluster	w	c	Note
A3733E	0.059 ± 0.002	0.33 ± 0.02	MD-CC
A3733W	0.037 ± 0.001	0.29 ± 0.02	MD-CC

The concentration degree of X-ray gas can be calculated from X-ray concentration parameter, which is highly essential in discriminating cool and non-cool core clusters. We estimated X-ray concentration parameters for each sub-structures by using the following equation provided by Santos et al. (2008).

$$c = \frac{S(r < 100 \text{ kpc})}{S(r < 500 \text{ kpc})}, \quad (3)$$

where S represents the surface brightness within 100 kpc and 500 kpc, respectively. We present the resulting X-ray morphological parameters in Table 4

3.5 Galaxy Cluster Mass Calculations

In hydrostatic equilibrium and isothermal spherical symmetry, galaxy cluster total mass can be estimated by adopting β model parameters (Lima Neto et al. 2003):

$$M(r) = \frac{3kT_0\beta r_c}{G\mu m_p} \times \left(\frac{r}{r_c}\right)^3 \times \left(1 + \left[\frac{r}{r_c}\right]^2\right)^{-1} M_\odot \quad (4)$$

Assuming an isothermal profile for galaxy clusters, r_Δ is given by Lima Neto et al. (2003):

$$r_\Delta = r_c \left(\frac{2.3 \times 10^8 \beta < kT >}{\Delta h_{70}^2 f^2(z, \Omega_M, \Omega_\Lambda) \mu r_c^2} \right), \quad (5)$$

where β is the shape parameter, r_c is the core radius given in kpc, $< kT >$ is the mean cluster temperature given in keV, and $f^2(z, \Omega_M, \Omega_\Lambda)$ is the redshift evolution of the Hubble parameter. Accordingly, the total X-ray mass of a galaxy cluster can be estimated from the scaling relations for comparison. Simulations and observations were confirmed the consistency of this approach (e.g., Ascasibar et al. 2006; Vikhlinin et al. 2006, 2009). The total mass of galaxy clusters is given by Vikhlinin et al. (2006):

$$H(z) \times M_{2500} = 1.25 \pm 0.05 \times 10^{14} \times \left(\frac{T_x}{5 \text{ keV}} \right)^{1.64 \pm 0.06} M_\odot, \quad (6)$$

where $H(z)$ is the Hubble parameter at redshift z . The $H(z)$ can be estimated from the following equation (Lima Neto et al. 2003):

$$H(z) = H_0 \times f(z, \Omega_M, \Omega_\Lambda). \quad (7)$$

The calculated total masses from the dynamical model and M - $< kT >$ relation are found to be highly consistent for our sample of cluster, and the estimated masses are presented in Table 5.

Table 5. The physical properties of A3733 system. The \star mark represents galaxy cluster mass estimations by adopting dynamical scaling relations, whereas the \diamond mark represents galaxy cluster mass results obtained from the beta model.

Parameter	A3733	A3733E	A3733W
z	0.0380	0.0368 ± 0.0002	0.0394 ± 0.0002
V_r (km s $^{-1}$)	11405	11044 ± 45	11825 ± 45
M_{2500}^\star ($10^{13} M_\odot$)	$11.19^{+1.04}_{-0.99}$	$4.85^{+0.62}_{-0.59}$	$6.34^{+0.85}_{-0.79}$
M_{2500}^\diamond ($10^{13} M_\odot$)	$14.35^{+3.17}_{-2.72}$	$6.24^{+1.67}_{-1.46}$	$8.11^{+2.70}_{-2.29}$

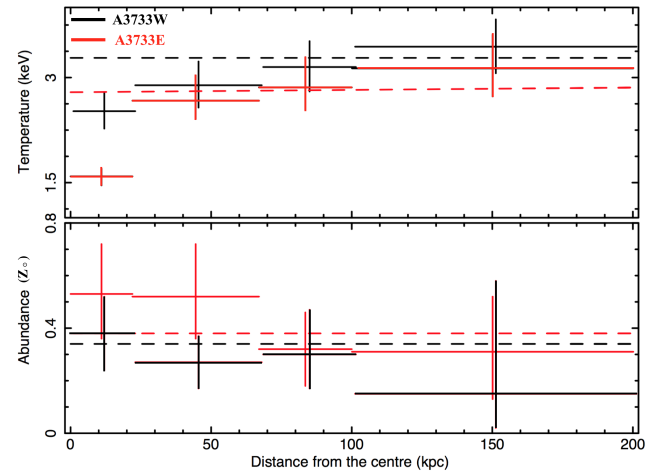


Figure 5. The spectral best-fit parameters of the radial profile of A3733, which were obtained by adopting four annular regions.

4 DISCUSSION

4.1 Sub-structures

The X-ray surface brightness map reveals the existence of two separated dense gas clumps in the A3733's cluster vicinity (Fig. 3). The eastern clump is concentrated on BCG1, whereas the western clump is concentrated on BCG2. Interestingly, optical galaxy density map demonstrates that the member galaxies are clustered around BCG2, and there is no nearby companion of BCG1 within 110 kpc radius (Fig. 1 and Fig. 2). The galaxy velocity histogram of A3733 is found to be roughly Gaussian (Fig. 1). X-ray and optical centroids of both BCGs coincide with each other with small positional offsets (< 1 kpc). The lack of positional offset between X-ray and optical centroids indicates a pre-merger scenario for A3733, and the cores of both sub-structures have not yet experienced a close core passage.

We additionally studied the surface brightness profiles of each sub-structures using the beta profile (Fig. 4). Previous X-ray investigations of galaxy groups and clusters have shown that galaxy clusters tend to have $\beta > 0.5$ (e.g., Mohr et al. 1999), whereas galaxy groups $\beta < 0.5$ (e.g., Mulchaey et al. 1996). The total X-ray mass of both structures are found to be $M_{2500} = 6.24^{+1.67}_{-1.46} 10^{13} M_\odot$ for A3733E and $M_{2500} = 8.11^{+2.70}_{-2.29} 10^{13} M_\odot$ for A3733W (see Table 5). By considering low beta ($\beta < 0.5$) and core radius ($r_c < 9$ kpc) and the low total X-ray mass, we identify both sub-structures as groups (Table 2). We additionally identify

A3733 as a small galaxy cluster due to its low X-ray total mass $M_{2500} = 1.44^{+0.32}_{-0.27} 10^{14} M_{\odot}$.

The mean ICM temperatures are estimated $2.79^{+0.21}_{-0.22}$ keV for A3733E and $3.28^{+0.27}_{-0.25}$ keV for A3733W, whereas the average abundance values are found to be $0.38^{+0.14}_{-0.12}$ and $0.34^{+0.13}_{-0.11}$ for A3733E and A3733W, respectively. The ICM temperature of connecting region is found to be slightly increased ($kT = 4.14$ keV). From the X-ray surface brightness distribution, a slight increase can be seen; however, there is still an absence of strong X-ray gas in between sub-structures (see Fig. 4 and Table 3). Therefore, we did not find a direct evidence of adiabatic compression of the gas.

The results of numerical simulations show a high temperature bar, which is almost perpendicular to the collision axis during the pre-assembling stages in the case of low impact parameters. However, the origin of hot region is not certain for pre-merger galaxy clusters. The hydrodynamic processes of heating a plasma are based on the viscous dissipation of energy in a form of the shock or adiabatic compression (Shaner & Gathers 1979; Schindler and Muller, 1993; Takizawa 1999; Ricker and Sarazin 2001). After the collision, the shock waves are mainly seen in the direction of the original collision axis and extending outwards (Feretti et al. 2002). The high speed shock waves are only observed with strong surface brightness discontinuities in the post-merger galaxy clusters (e.g., Markevitch et al. 2002; Botteon et al. 2016; Dasadia et al. 2016); however, such strong discontinuities have not been seen in the pre-merger galaxy clusters (e.g., Caglar 2018). For the A3733 system, we speculate that the hot region in between sub-structures can be due to shock-heating, even though we did not see any strong discontinuity in the surface brightness profile. But, we note that further investigations are required to understand the origin of hot region in between sub-structures.

To understand the disturbance level of gas, we separately estimate the X-ray morphological parameters for both sub-structures. Due to the high centroid shifts ($w > 0.035$), we identify both sub-structures as moderately disturbed systems. These results indicate that the merging process has already started. Additionally, the resulting X-ray concentration parameters are found to be $c \sim 0.3$ for each sub-structure. Santos et al. (2008) reports that cool core hosting galaxy clusters tend to have $c > 0.15$. Due to high X-ray morphological parameters of A3733E ($c = 0.33$) and A3733W ($c = 0.29$), we identify both sub-structures as cool cores. Additionally, the projected X-ray temperature profiles of A3733E and A3733W demonstrate the existence of cool centres relative to their surroundings (see Fig. 5). These results also imply that the centres of both sub-structures have not yet experienced any crucial events that can destroy or dislocate their cool centres. Therefore, we identify the galaxy cluster A3733 as a pre-merger candidate. We present the X-ray morphological parameters results in Table 4.

4.2 The Dynamical Model of The A3733 System

The Newtonian gravitational binding criterion can be applied to understand binding state of A3733. The criterion gives binding probabilities of two-body systems and estimates approaching speed, collision time and relative distance between two-body systems. This model successfully explained binding state of different two-body systems in the

literature (e.g., Beers et al. 1982; Cortese et al. 2004; Hwang & Lee 2009; Yan et al. 2014; Andrade-Santos et al. 2015; Nascimetro et al. 2016; Bulbul et al. 2016; Caglar & Hudaverdi 2017). The solution of the Newtonian binding criterion describes the binding state of a system in four solutions: two bound incomings (BI), a bound outgoing (BO) and an unbound outgoing (UO).

The Newtonian criterion for gravitational binding of two-body systems can be solved from the following equation:

$$V_r^2 R_p \leq 2GM \sin^2 \alpha \cos \alpha, \quad (8)$$

where V_r is the radial velocity difference, R_p is the projected separation, G is the gravitational constant, and α is the projection angle. The parametric equation solves the projection angle α for each radial velocity difference V_r . The radial velocity and the projected separation are related to the projection angle of system:

$$V_r = V \sin \alpha, R_p = R \cos \alpha, \quad (9)$$

where V and R are the three dimensional velocity difference and separation of the two-body system in the field of sky, respectively. The parametric motion equation of bound system can be estimated from the following equations:

$$t = \left(\frac{R_m^3}{8GM} \right)^{1/2} (\chi - \sin \chi), \quad (10)$$

$$R = \frac{R_m}{2} (1 - \cos \chi), \quad (11)$$

$$V = \left(\frac{2GM}{R_m} \right)^{1/2} \frac{\sin \chi}{(1 - \cos \chi)}, \quad (12)$$

where R is the separation at time t , R_m is the separation at the maximum expansion, M is the total mass of the system, and χ is the development angle.

For gravitational unbound systems:

$$t = \frac{GM}{V_{\infty}^3} (\sinh \chi - \chi), \quad (13)$$

$$R = \frac{GM}{V_{\infty}^2} (\cosh \chi - 1), \quad (14)$$

$$V = V_{\infty} \frac{\sinh \chi}{(\cosh \chi - 1)}, \quad (15)$$

where V_{∞} is the expansion velocity at the asymptotic limit.

The relative probabilities of the solutions can be estimated using the formula:

$$p_i = \int_{\alpha_{inf,i}}^{\alpha_{sup,i}} \cos \alpha \, d\alpha, \quad (16)$$

where i represents i -th solution of possible binding scenarios. The resulting probabilities were normalised by $P_i = p_i / (\sum_i p_i)$ in our calculations.

The following parameters of A3733 were used in the solutions: the radial velocity difference of $V_r = 781 \pm 64$ km s⁻¹, the projected distance $R_p = 250$ kpc, a total mass of $M_{200} = 1.435 \times 10^{14} M_{\odot}$, and the age of the universe at cluster redshift $t = 12.96$ Gyr (4.09×10^{17} s). The resulting solution of the Newtonian gravitational binding criteria of A3733

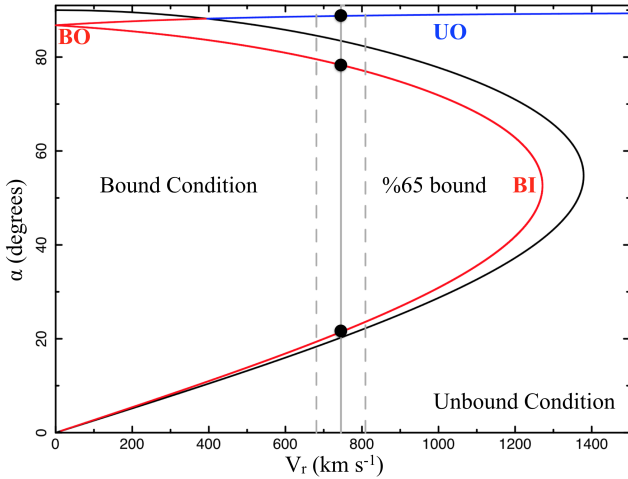


Figure 6. The projection angle (α) as a function of the relative radial velocity difference (V_r) of the sub-structures A3733W and A3733E. BI, BO and UO stand for Bound-Incoming, Bound-Outgoing, and Unbound-Outgoing solutions. The Red and the blue lines represent the bound and the unbound solutions, respectively. The black curve represents the limit of bound solutions due to the Newtonian criterion. The gray vertical lines demonstrates the relative radial velocity $V_r = 781 \pm 64 \text{ km s}^{-1}$.

Table 6. The estimated parameters for bound incoming solutions of the two-body dynamical model.

χ (rad)	α (degrees)	R (Mpc)	R_m (Mpc)	V (km s^{-1})	P (%)
4.92	77.58	1.16	2.92	763	11.7
5.65	22.63	0.27	2.81	1936	88.2

is presented in Fig. 6. Solving the equation 8, the system is found to be % 65 bound. In addition, the parametric solution gives three solutions for A3733: two bound in-comings and an unbound outgoing (see Fig. 6). The first solution (% 11.7 probability) indicates that A3733E and A3733W have 3D separation $R = 1.16 \text{ Mpc}$ and approach each other with colliding velocity $V = 763 \text{ km s}^{-1}$. The high probable ($P = \% 88.2$) scenario suggests that the cores of sub-structures have a 3D separation of 0.27 Mpc and will collide in 0.14 Gyr with the relative in-falling velocity of 1936 km s^{-1} . The unbound scenario (% 0.01 probability) results in 3D separation of 12.0 Mpc . The parameters of parametric solutions are presented in Table 6 and 7. We note that, as mentioned in Andrade-Santos et al. (2015), the solution of this method does not involves angular momentum of the system due to absence of angular momentum information of the colliding structures.

4.3 Brightest Cluster Galaxies

A3733 hosts two binary galaxy groups, which are concentrated on two different BCGs (NGC 6998 for A3733W and NGC 6999 for A3733E). The velocity histogram of galaxies can be fitted with a single Gaussian model; however, the region around NGC 6998 appears to be crowded with mem-

Table 7. The estimated parameters for unbound outgoing solution of the two-body dynamical model.

χ (rad)	α (degrees)	R (Mpc)	V (km s^{-1})	V_∞ (km s^{-1})	P (%)
3.08	88.81	12.0	745	680	0.01

ber galaxies, whereas NGC 6999 has no companion within 110 kpc radius (Fig. 2 and Fig. 1). The X-ray centroids of both BCGs coincide with the optical centroids with a displacement of less than 1 kpc . The X-ray and optical association are estimated using the following equation, which is explained in detail by Pineau et al. (2011)

$$LR(r) = \frac{1}{2\lambda} e^{-0.5r^2}, \quad (17)$$

where LR is the likelihood ratio of association, λ is the pilot function, r is the distance between X-ray and optical centroids. The resulting LR values are found to be % 96, % 88 for NGC 6998 and NGC 6999, respectively.

4.3.1 NGC 6998

NGC 6998 is the second brightest galaxy in the vicinity of A3733 (Postman & Lauer 1995). The diffuse ($\sim 400 \text{ kpc}$) radio emission, which comes from the central black hole is associated with NGC 6998 (Morganti et al. 1999). In Figure A1, the radio lobes and a strong jet can also be seen from the GMRT 150 MHz and VLA 1400 MHz image. The X-ray spectrum of NGC 6998 was fitted with thermal and power law component by adopting a redshift dependent fixed nH density of this source ([apec+powerlaw]*ztbabs). Based on the fit, we obtained the X-ray luminosity $\log L_x = 41.75 \text{ erg s}^{-1}$ and the hardness ratio $HR = 0.55 \pm 0.04$. We note that the hardness ratio is estimated using the following formula $HR = H-S/H+S$, where H is count rate in $2.0-10.0 \text{ keV}$ and S is count rate in $0.5-2.0 \text{ keV}$ (Caglar & Hudaverdi 2017). Therefore, we identify this source as the low luminosity active galactic nuclei.

4.3.2 NGC 6999

NGC 6999 is the brightest galaxy of A3733 (Postman & Lauer 1995) and it has no nearby companion within 110 kpc radius. The X-ray spectra of this source is well-modelled with a single thermal model with a fixed nH density value (apec*tbabs). The resulting X-ray luminosity is obtained as $\log L_x = 40.80 \text{ erg s}^{-1}$ for this source.

5 SUMMARY

In this study, X-ray and optical data were used to perform structural analysis of A3733. The obtained features indicate that A3733 is a bimodal system, which is in an early stage of merger. The main findings of the study are summarized as follows:

- The optical density map reveals the existence of dense region around the BCG2. Moreover, the velocity histogram of member galaxies results in two peak points, which gives an impression of clustering around both BCGs (see Fig. 1).

- A3733E is concentrated at the BCG1, and A3733W is concentrated at the BCG2. While X-ray centroid of the BCG1 is dislocated from optical centroid by ~ 1 kpc, X-ray centre of the BCG2 matches with its optical centre (see Fig. 2).

- The average temperature values of A3733E and A3733W are found to be 2.79 keV and 3.28 keV, respectively (see Table 3).

- The both sub-structures are found to host cool cores (see Fig. 5, Table 4).

- The mass calculations result in $M_{2500} = 6.24 \times 10^{13} M_{\odot}$ for A3733E and $M_{2500} = 8.11 \times 10^{13} M_{\odot}$ for A3733W (see Table 5).

- The surface brightness profile of A3733 reveals an absence of strong X-ray emitting gas between sub-structures (see Fig. 4).

- The high probable (% 88.2) dynamical binding model suggest that the cores of sub-structures have a 3D separation of 0.27 Mpc and will collide in 0.14 Gyr with the relative infalling velocity of 1936 km s^{-1} (see Table 6).

In this work, we find some pieces of evidence that A3733 is a pre-merger system due to the following signatures; a) X-ray and optical centres of BCGs substantially coincide with each other, b) the gas within sub-structures' cores are not disturbed, c) there is an absence of a strong X-ray emitting gas between two sub-structures, d) both sub-structures are found to host cool cores, e) the ICM temperature between sub-structures is slightly increased ($kT = 4.14 \text{ keV}$). In conclusion, the system is clearly at the early stage of the merger. For future research, this study encourage a longer exposure X-ray observation and comparisons with numerical simulations.

ACKNOWLEDGEMENT

Authors would like to thank anonymous referee for his valuable comments and suggestions. Authors are grateful to Gözde Özzeybek for her feedbacks and comments. TC also would like to thank Reinout van Weeren, Aurora Simionescu, Gabriella Di Gennaro, Dilovan Serindag and Henk Hoekstra for very useful discussions.

REFERENCES

Andrade-Santos F. et al., 2015, *ApJ*, 803, 108
 Arnaud K. A., 1996, *ApJ*, 101, 17
 Akamatsu H. et al., 2016, *A&A*, 593, 7
 Akamatsu H. et al., 2017, *A&A*, 606, 1
 Ascasibar Y., Sevilla R., Yepes G., Müller V., Gottlöber S., 2006, *MNRAS*, 371, 193
 Baier F. W., Gastao B., Lima Neto, Whiper H., 1996, in Coles P., Martinez V. J., Pons-Borderia M.-J., eds, *ASP Conf. Ser. Vol. 94. Mapping Measuring and Modelling the Universe. Astron. Soc. Pac., San Francisco*, p. 215
 Beers T. C., Geller M. J., Huchra J. P., 1982, *ApJ*, 257, 23
 Botteon A., Gastaldello F., Brunetti G., Kale R., 2016, *MNRAS*, 463, 1534

Botteon A. et al., 2018, *MNRAS*, 478, 885
 Bulbul E. et al., 2016, *ApJ*, 818, 131
 Caglar T., Hudaverdi M., 2017, *MNRAS*, 471, 4990
 Caglar T., Hudaverdi M., 2017, *MNRAS*, 472, 2633
 Caglar T., 2018, *MNRAS*, 475, 2870
 Cavaliere A., Fusco-Femiano R., 1976, *A&A*, 49, 137
 Condon J. J. et al., 1998, *AJ*, 115, 1693
 Cortese L., Gavazzi G., Boselli A., Iglesias-Paramo J., Carrasco L., 2004, *A&A*, 425, 429
 Dasadia S., Sun M., Sarazin C., Morandi A., Markevitch M., Wik D., Feretti L., Giovannini G., Govoni F., Vacca V., 2016, *ApJ*, 820, 20
 Dalton G. B., Efstathiou G., Maddox S. J., Sutherland W. J., 1994, *MNRAS*, 269, 151
 Di Gennaro G. et al., 2019, preprint (arXiv:1902.00235)
 Ebeling H., Voges W., Bohringer H., Edge A. C., Huchra J. P., Briel U. G., 1996, *MNRAS*, 281, 799
 Feretti L., Gioia I., M., Giovannini G., *MERGING PROCESSES IN GALAXY CLUSTERS* Springer Netherlands, 2002, 272, pp 140-141
 Feretti L., Giovannini G., Govoni F., Murgia M. 2012, *A&ARv*, 20, 54
 Fujita Y., Koyama K., Tsuru T., Matsumoto H., 1996, *PASJ*, 48, 191
 Fujita Y., Tawa N., Hayashida K., Takizawa M., Matsumoto H., Okabe N., Reiprich T. H., 2008, *PASJ*, 60, 343
 Gutierrez K. & Krawczynski H., 2005, *ApJ*, 619, 161
 Hallman E. J., Alden B., Rapetti D., Datta A., Burns J. O., 2018, *ApJ*, 859, 44
 Hickox R. C., Markevitch M., 2006, *ApJ*, 645, 95
 Hwang H. S., Lee M. G., 2009, *MNRAS*, 397, 2111
 Intema H. T., Jagannathan P., Mooley K. P., Frail D. A., 2017, *A&A*, 598, 78
 Jones D. H. et al., 2009, *MNRAS*, 399, 683
 Katgert P., Mazure A., den Hartog R., Adami C., Biviano A., Perea, J., 1998, *A&AS*, 129, 399
 Kato Y., Nakazawa K., Gu L., Akahori T., Takizawa M., Fujita Y., Makishima K., 2015, *PASJ*, 67, 71
 Kolokotronis V., Basilakos S., Plionis M., Georgantopoulos I. 2001, *MNRAS*, 320, 49
 Lima Neto G. B., Capelato H. V., Sodr  L., Jr. Jr. Proust D., 2003, *A&A*, 398, 31
 Markevitch M., Ponman, T. J., Nulsen, P. E. J., et al. 2000, *ApJ*, 541, 542
 Markevitch M. et al., 2002, *ApJ*, 567, 27
 Markevitch M., Vikhlinin A., 2007, *PhR*, 443, 1
 Mulchaey J. S., Davis D. S., Mushotzky R.F., Burstein D., 1996, *ApJ*, 456, 80
 Mohr J. J., Evrard A. E., Fabricant D. G., Geller M. J., 1995, *ApJ*, 447, 8
 Mohr J. J., Mathiesen B., Evrard A. E., 1999 *ApJ*, 517, 627
 Morganti R., Oosterloo T., Tadhunter C. N., Aiudi R., Jones P., Villar-Martin M., 1999, *A&AS*, 140, 355
 Nascimento R. S., Ribeiro A. L. B., Lopes P. A. A., 2016, *MNRAS*, 464, 183
 Piffaretti R., Arnaud M., Pratt G. W., Pointecouteau E., Melin, J. B., 2011, *A&A*, 534, 109
 Pineau F.-X., Motch C., Carrera F., Della Ceca R., Derrie re S., Michel L., Schwobe A., Watson M. G., 2011, *A&A*, 527, 126
 Postman M., Lauer T. R., 1995, *ApJ*, 440, 28
 Press, W. H., & Schechter, P. 1974, *ApJ*, 187, 425
 Ricker, P., M., Sarazin, C. L., *Off-Axis Cluster Mergers: Effects of a Strongly Peaked Dark Matter Profile*, 2001, *ApJ*, 561, pp 621-644
 Robertson J. G., Roach G. J., 1990, *MNRAS*, 247, 387
 Santos J. S., Rosati P., Tozzi P., B  hringer H. Ettori S., Bignamini A., 2008, *A&A*, 483, 35
 Sarazin C. L., 2002, in Feretti L., Gioia I. M., Giovannini

- G., eds, *Astrophysics and Space Science Library* Vol. 272, Merging Processes in Galaxy Clusters. pp 1-38 (arXiv:astro-ph/0105418), doi:10.1007/0-306-48096-4 1
- Sarazin, C. L., Finoguenov, A., Wik, D. R., 2013, *AN*, 334, 346
- Schmidt W., Byrohl C., Engels J. F., Behrens C., Niemeyer J. C., 2017, *MNRAS*, 470, 142
- Schindler and Muller, (1993), *A&A*, 305, 756
- Shaner J. W. & Gathers G. R., in *High Pressure Science and Technology*, ed. K. D. Timerhous (Plenum, New York, 1979), pp. 847-867
- Smith R.K., Brickhouse N.S., Liedahl D.A., Raymond J.C., 2001, *ApJ*, 556, L91
- Smith R. J. et al., 2004, *AJ*, 128, 1558
- Solanes J. M., Stein P., 1998, *A&AS*, 131, 221
- Stein P., 1996, *A&AS*, 116, 203
- Stein P., 1997, *A&A*, 317, 670
- Takizawa, M., Two-temperature intracluster medium in merging clusters of galaxies, *Astron. Nachr.*, 1999, 320, pp 4-5
- Vikhlinin, A., Kravtsov, A., Forman, W., Jones, C., Markevitch, M., Murray, S. S., Van Speybroeck, L., 2006, *ApJ*, 640, 691
- Vikhlinin A. et al., 2009, *ApJ*, 692, 1033
- Werner, N., Finoguenov, A., Kaastra, J. S., Simionescu, A., Dietrich, J. P., Vink, J., Böhringer, H. 2008, *A&A*, 482, 29
- West M. J., Villumsen J. V., Dekel A. 1991, *ApJ*, 369, 287
- Wilms, J.; Allen, A.; McCray, R., 2000, *ApJ*, 542, 914
- Wright A. E., Griffith M. R., Burke B. F., Ekers R. D., 1994, *ApJS*, 91, 111
- Yan P., Yuan Q., Zhang L., Zhou X., 2014, *APJ*, 147, 106
- Zuhone, J. A., 2011, *ApJ*, 728, 54

APPENDIX A: RADIO IMAGES

We present the radio images, which are obtained from the *GMRT* 150 MHz all-sky radio survey, The *NRAO VLA* 1400 MHz sky survey and The *Green Bank* 4850 MHz sky survey. The absence of diffuse synchrotron emission in the form of radio halo or relics, which were only observed in post-merger galaxy clusters (e.g., Di Gennaro et al. 2019), also supports pre-merger scenario indirectly for A3733 (see Fig. A1).

This paper has been typeset from a \LaTeX file prepared by the author.

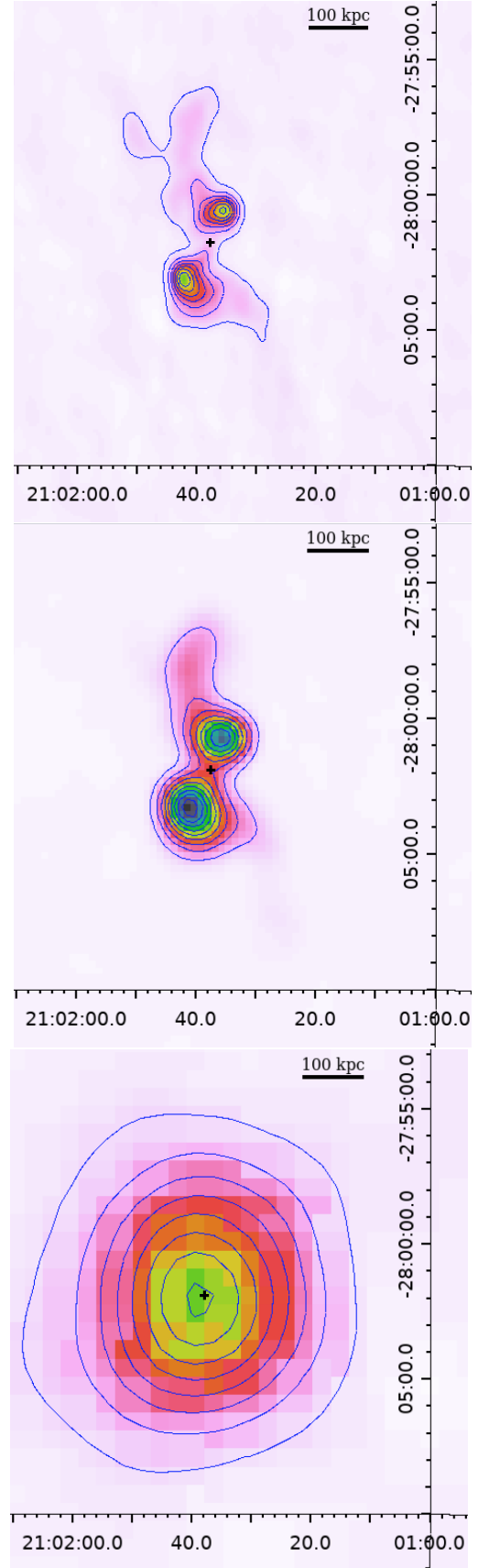


Figure A1. The radio data **Top:** GMRT 150 MHz all-sky radio survey; **Middle:** The NRAO VLA 1400 MHz sky survey; **Bottom:** The *Green Bank* 4850 MHz sky survey. The black plus signs demonstrate the position of BGC2.